HELMHOLTZ
ZENTRUM BERLIN
für Materialien und Energie

Permanent Magnets
Including Wigglers and Undulators
Part II

Johannes Bahrdt

June 20th-22nd, 2009

Part II

Metallurgic aspects of permanent magnets
Magnetic domains
Observation techniques of magnetic domains
New materials
Aging / damage of permanent magnets
Simulation methods
PPM quadrupoles

Crystal Structure of RE-Permanent Magnets I

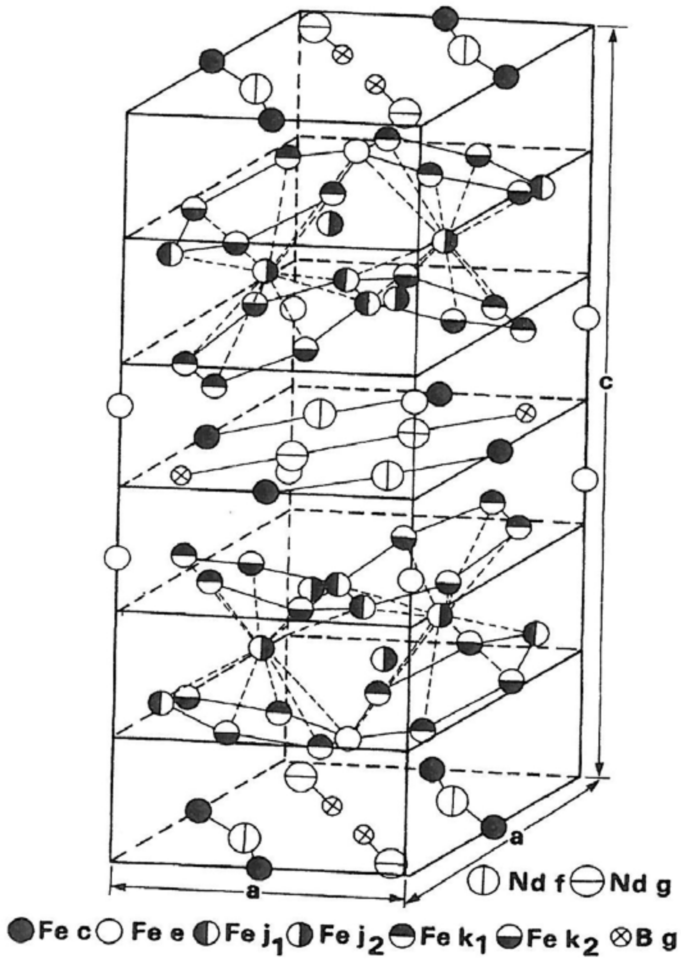

Unit cell of tetragonal
$Nd_2Fe_{17}B$
in reality the ratio c/a is smaller

The Fe layers couple antiferromagnetically to the Nd, B layers

Partial substitution of Nd with Dy
→ crystal anisotropy increases
coercivity increases

Dy atoms couple antiparallel
→ saturation magnetization
decreases simultaneously

J. Herbst, Review of Modern Physics, Vol. 63, No. 4 (1991) p819.

Crystal Structure of RE-Permanent Magnets II

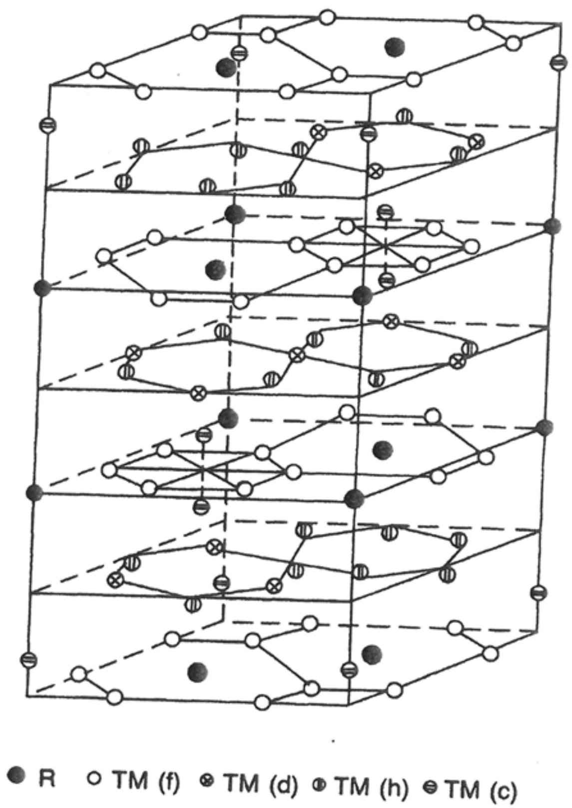

Unit cell of rhombohedral
Sm_2Co_{17} (R=Sm Tm=Co)

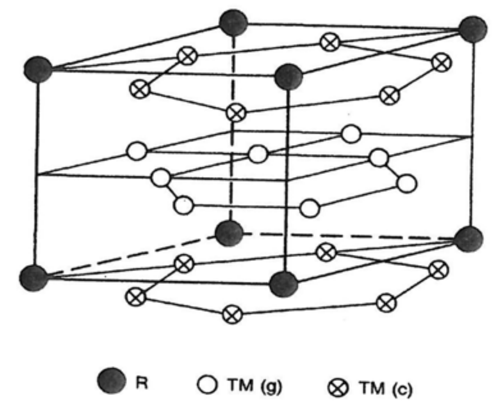

Unit cell of the hexagonal
$SmCo_5$ (R=Sm Tm=Co)

J. Herbst, Review of Modern Physics, Vol. 63, No. 4 (1991) p819.

Metallurgy: Theoretic Limits of Magnet properties

Theoretical limit of energy product:

$$(BH)_{\max} = B_r^{\ 2} / \mu$$

$$B_r(20°C) = B_{r-sat}(20°C) \cdot \frac{\rho}{\rho_0} \cdot (1 - V_{nonmagnetic}) \cdot f_\varphi$$

$$f_\varphi = \cos(\varphi)$$

$$\varphi = \arctan\left(2 \frac{B_{r-perp}}{B_{r-par}} \right)$$

Typical values for sintered NdFeB magnets

$\frac{\rho}{\rho_0} \geq 99\%$ due to liquid phase sintering

$f_\varphi \geq 98\%$ alignmnet coefficient for isostatic pressing

< 2.5 wt.% of impurities like Nd-oxide
requires vacuum induction furnace and inert gas processing
< 2.5 wt.% of RE constituents ⇨ $V_{nonmagnetic} < 0.05$

➡ theoretic limit: 63 MGOe (achieved: 59 MGOe)

Typical Structure of Sintered NdFeB Magnets

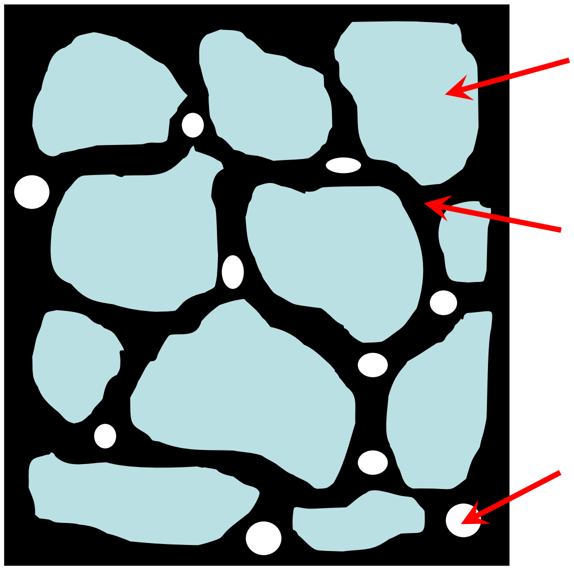

$Nd_2Fe_{14}B$ grains (monocrystalline)

RE rich constituents containing
Nd, Co, Cu, Al, Ga, Dy (area is exaggerated)

Nd oxides

$Nd + H_2O \Longrightarrow NdOH + H$

$H + Nd \Longrightarrow NdH$

appropriate chemical
additions between grains
avoid Hydrogen decrepitation

The interesting effects
happen at the boundaries!

Hydrogen decrepitation destroys magnetic material
- fatal for magnets in operation
- ecologically interesting for decomposition and RE recovery

Coercivity

In the bulk magnetic domains are separated by Bloch walls:

below a certain size: no Bloch walls can exist due to energetic considerations
above that size several domains in one particle are possible
critical size for Fe: 0.01 μm, for Ba ferrite: 1 μm
above that size remanence and coercivity follow roughly a 1/size dependence
RE-magnets have typical grain sizes that are a bit larger than single domain size

normally, the rotation of the magnetization vector occurs in the boundary plane
In thin films: Neel walls, magnetization vector rotates perpendicular to boundary

Reason for coercivity:

- intentionally introduced imperfections (e.g. carbides in steel magnets) impede the movement of Bloch walls
- stable single domain grains which can be switched only completely
- introduction of anisotropy

Basically two types of anisotropy:

- shape of microscopic magnetic parts in non magnetic matrix (needles etc)
- crystal anisotropy

Two Classes of Magnets

A) Small particle magnets with shape anisotropy

shaped magnetic material in non magnetic matrix
e.g. FeCo in less magnetic FeNiAl (AlNiCo) or nonmagnetic lead matrix

Shape anisotropy of AlNiCo 5:
Spinodal decompostion
energy product largest along direction of needles (factor of 10 as compared to perpendicular direction)

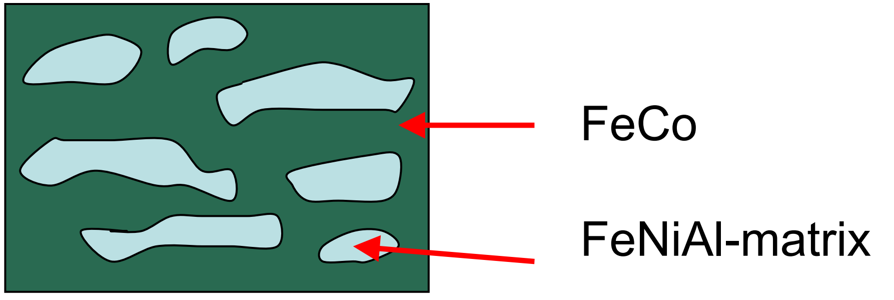

B) Small particle magnets with crystalline anisotropy

- **Nucleation type, e.g. $SmCo_5$, $Nd_2Fe_{14}B$, ferrites**
  easy motion of domain walls within one domain;
  motion impeded at grain walls

- **Pinning type, e.g. $Sm(Co, Fe, Cu, Hf)_7$, $SmCo_5$ + Cu precipitation, Sm_2Co_{17} with $SmCo_5$ precipitation (size of domain wall thickness)**
  Domain walls are pinned to boundaries of precipitations

Initial Magnetization

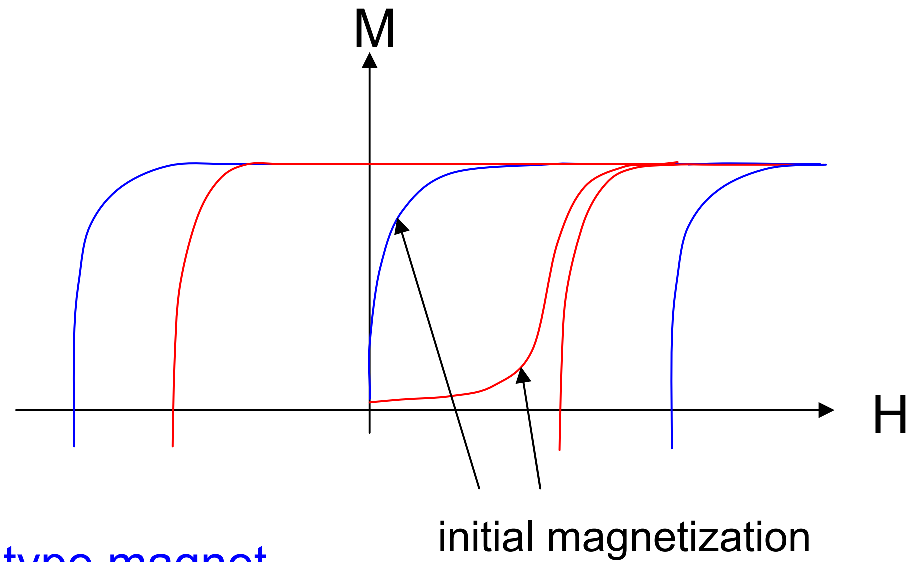

Nucleation type magnet

directly after heating: many domain walls inside each grain
Bloch walls are rather freely movable within grains
high initial permeability; walls are pushed out of grain bulk at first magentization
fixing of walls at the grain boundaries
usually no domain walls within grain bulk under fully magnetized conditions
in reverse field most grains switch completely the magentization

Pinning type magnet

pinning centers inside grains impede wall movement
high fields are required to move the walls

Metallurgy I: Coercivity Versus Grain Size

Partial replacement of Nd with Dy enhances the anisotropy field and thus the coercivity, however:

Dy is expensive & remanence is reduced

Use all means to enhance coercivity without Dy, e.g. optimizing the grain size
Systematic studies show:
Within the grain size range of 3.9 and 7.6 µm
the coercivity H_{cj} increases with smaller grain size

$$H_{cj}(20°C) \propto (grainsize)^{-0.44}$$

Powder size µm	Grain size µm	Hcj (20° C) kA/m	Hcj (100° C) kA/m
1,9	3,8	1178	581
2,2	4,3	1162	573
2,6	4,9	1090	525
3,0	6,0	971	462
3,5	7,6	883	414

K. Uestuener, M. Katter, W Rodewald, 2006

Metallurgy II: Remanence and Coercivity Versus Alignment Angle and External Field Direction

with inreasing alignment coefficient:
- remanence increases
- coercivity decreases

W. Rodewald et al., VAC, Hagener Symposium für Pulvermetallurgie, Band 18 (2002) pp 225 -245.

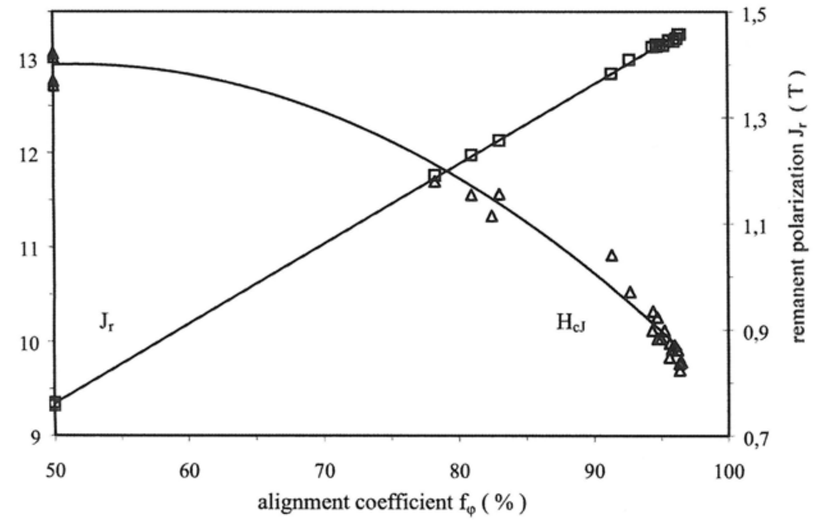

dependence of coercivity on applied external field direction:

rough approximation: $$H_{cj} \propto \frac{1}{\cos(\theta)}$$

detailed study at 0°, 45° 90° shows:

- nearly no difference between 0° and 45°
- increase of Hcj by - 30% for axially pressed material
  - 70% for isostatically pressed material

in specific cases this enhancement of coercivity can be used.

M. Katter Transactions on Magnets, Vol: 41, No:10, (2005)

HELMHOLTZ ZENTRUM BERLIN für Materialien und Energie

Linear superposition of PPM fields works within a few percent.
For higher accuracy non unity of permeability has to be regarded.

μ_{par} depends on fabrication process
1.05 axially pressed
1.03 isostatically pressed
no correlation with coercivity

μ_{perp} decreases with increasing coercivity
1.17 (H_{cj}=18kOe), 1.12 (H_{cj}=32kOe)

M. Katter Transactions on Magnets, Vol: 41, No:10, (2005) Study of grain size growth with ASTM E112

(ASTM E112 is a standard for grain size measurement)

the grain radius inceases over time approximately with

$$R(t) = k \cdot t^{1/n}$$

n = 2-4 for pure metals

n = 16-20 for sintered NdFeB with B < 5.7at.%

n = 7.5 for sintered NdFeB magnets with B > 5.7 at.%

n = 10 for sintered NdFeB magnets with RE-contituents > 4wt.%

sintering time has to be adjusted appropriately

to achieve an optimum grain size of 3-5μm and to avoid giant grains

NdFeB has hexagonal structure

Distribution of numbers of corners changes during sintering

optimization of six corner grains

Grains in a sintered NdFeB magnet,
averaged grain size: 4.6μm;
polished and chemical etched surface as
seen with a conventional light microscope

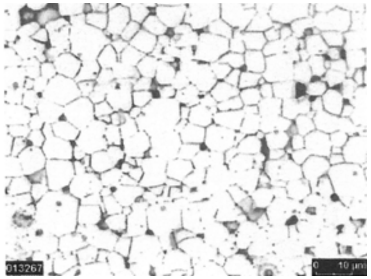

Courtesy of VAC

HELMHOLTZ ZENTRUM BERLIN für Materialien und Energie

Bitter Patterns

Ferrofluids: fine magnetic grains (a few tens of nm) in a colloid suspension is spread on a polished surface of a magnetic sample magnetic grains are attracted at the domain walls

Resolution: 100nm

Magnetooptical effects:

- Kerr-effect (MOKE), reflection geometry
- Faraday-effect, transmission geometry

Resolution: 150nm, suitable for the detection of fast processes

All magnetooptical effects can be described with a generalized dielectric permittvity tensor which reduces for cubic crystals to:

$$\vec{\varepsilon} = \varepsilon \begin{pmatrix} 1 & -iQ_V m_3 & iQ_v m_2 \\ iQ_v m_3 & 1 & -iQ_v m_1 \\ -iQ_v m_2 & iQ_v m_1 & 1 \end{pmatrix} + \begin{pmatrix} B_1 m_1^2 & B_2 m_1 m_2 & B_2 m_1 m_3 \\ B_2 m_1 m_2 & B_1 m_2{}^2 & B_2 m_2 m_3 \\ B_2 m_1 m_3 & B_2 m_2 m_3 & B_1 m_3^2 \end{pmatrix}$$

Similarly, a magnetic permeability tensor can be set up, however, the coefficients are 2 orders of magnitude smaller and usually neglected

Inserting these tensors into Fresnel's equation describes all effects

Methods of Magnetic Domain Measurement II

Geometries of magnetooptical Kerr- and Farady-effect

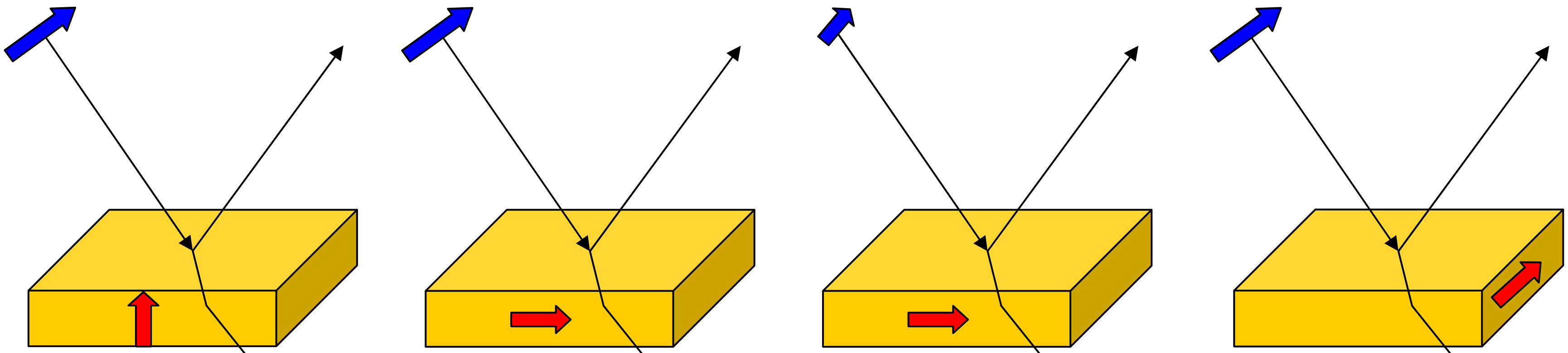

polar magnetization
parallel to plane of inc.
rotation of reflected
and transmitted light
clockwise

longitudinal magn.
parallel
rotation of reflected
and transmitted light
counter clockwise

longitudinal magn.
perpendicular
Kerr: clockwise
Faraday:
counter clockwise

transverse magn.
parallel
Kerr: same direction
change of amplitude
Farady: no effect in transm.

- linearly polarized light forces charges to vibrational motion
- moving charges experience Lorentz forces
- the additional vibrational motion introduces perpendicaular electric field component in reflected / transmitted beam

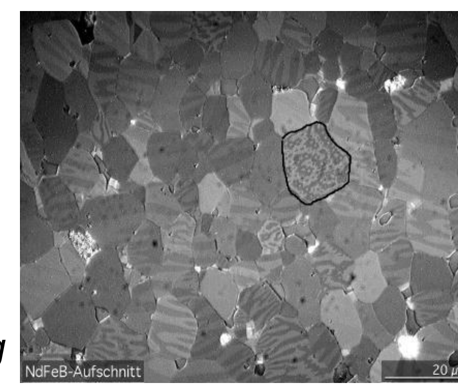

http://upload.wikimedia.org/wikipedia/commons/b/b4/NdFeB-Domains.jpg

X-Ray Magnetic Circular Dichroism (XMCD)

Different absorption coeffficients of right / left handed circularly polarized light

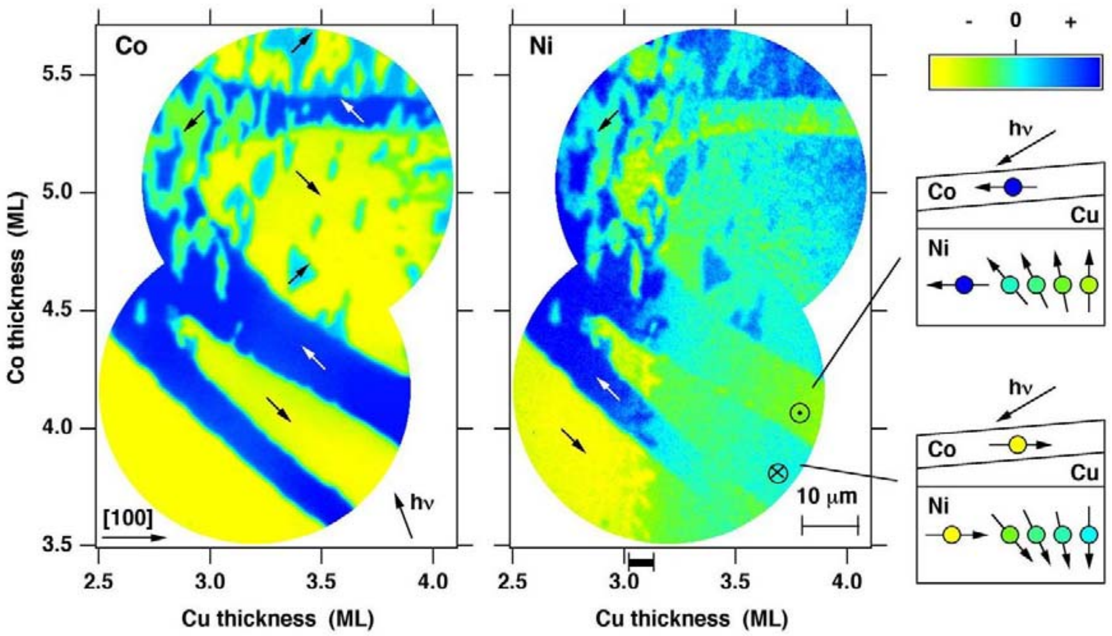

W.Kuch et al., Phys. Rev. B, Vol 65, 0064406-1-7 (2002)

Photoelectron emission microscope (PEEM) at BESSY UE56 APPLE

Exchange coupling between magnetic films of Co and Ni separated by a nonmagnetic layer of Cu with variable thickness

X-Ray Holography

No lenses or zone plates are needed

resolution 50nm demonstrated so far

Principle:

absorption of coherent cicularly polarized light within an aperture of 1.5µm

reference hole 100-350nm (conical)

coherent overlap of both beams

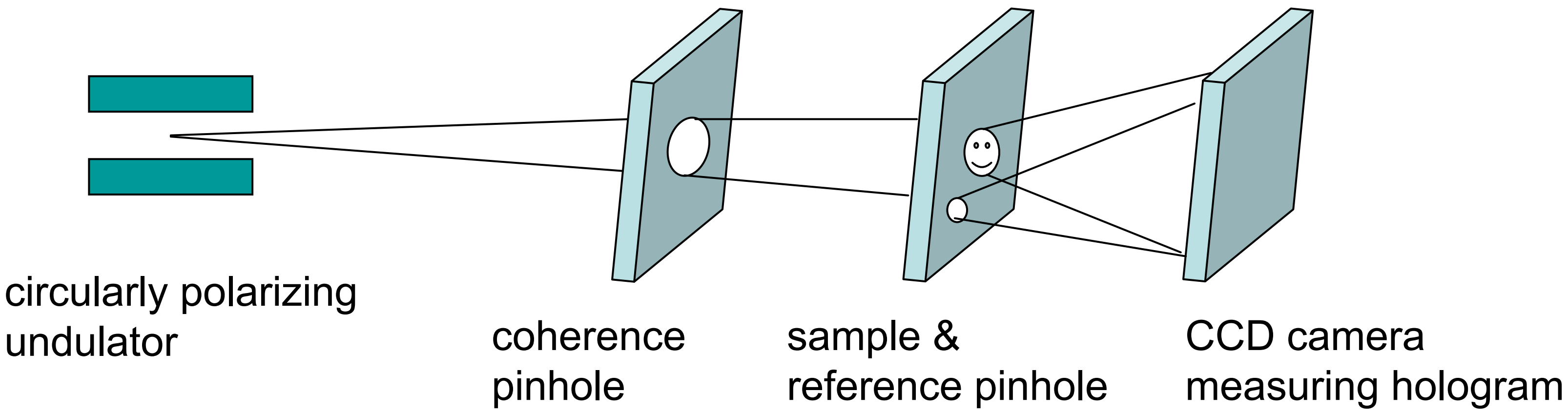

S. Eisebitt et al, Phys. Rev. B 68, 104419-1-6 (2003)

S. Eisebitt at al, Nature Vol. 432 (2004) pp 885-888

Neutron decoherence imaging

advantage: thick samples (cm range) can be studied

disadvantage: resolution so far 50-100 µm

Principle:

coherent neutrons from source grating (de Broglie waves)

diffraction of neutrons at magnetic domain walls, distortion of wavefront

Talbot image of distorted wavefront using phase grating

detection of talbot image with sliding absorption grating and detector

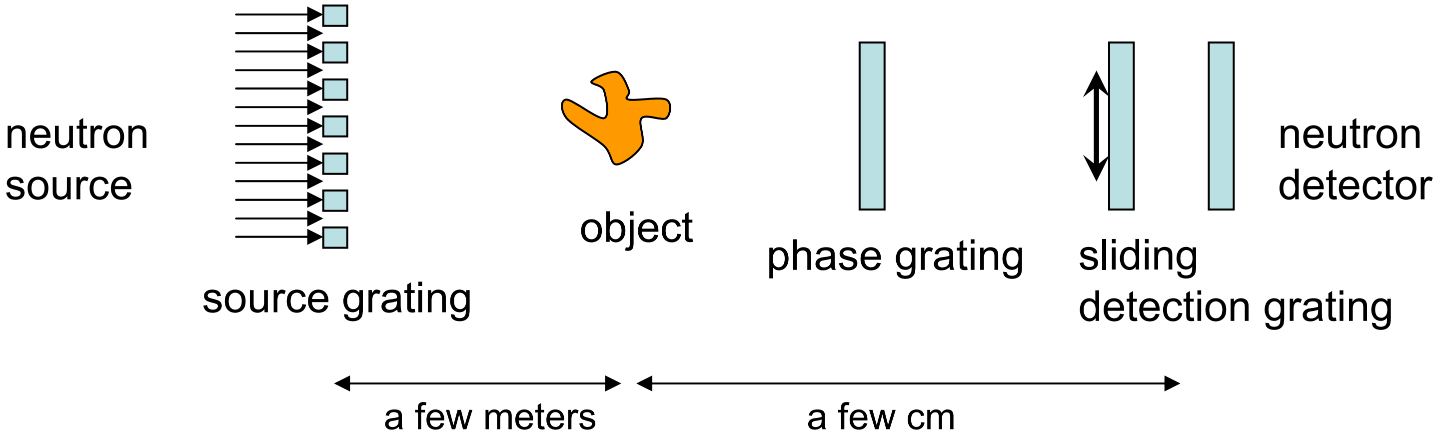

F. Pfeiffer et al., Phys. Rev. Let. 96. 215505-1-4, 2006

C. Grünzweig et al., Phys. Rev. Let. 101, 025504, 2008

Transmission electron microscope
Lorentz force microscopy, resolution 10nm

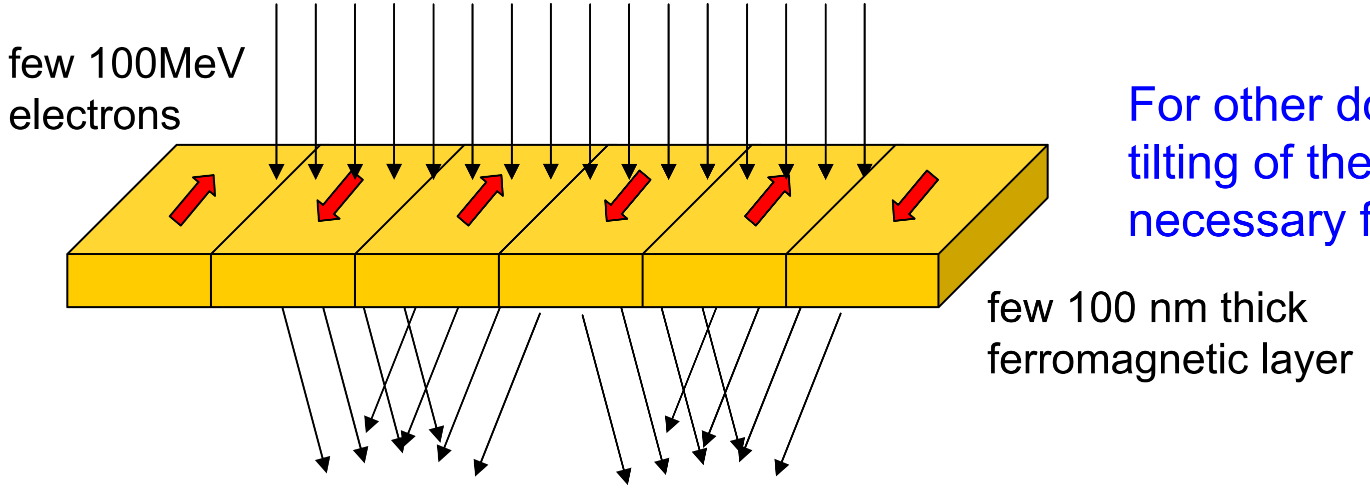

For other domain geometries tilting of the sample may be necessary for a net deflection

Further methods
XMCD in absorption or transmission geometry
Low energy electron diffraction (LEED)
Magnetic force microscope (resolution 10nm)
Spin polarized scanning tunneling microscope (resolution 1nm)

See also: A. Hubert, R. Schäfer, „Magnetic Domains", Springer-Verlag, Berlin, Heidelberg, New York, 2000

Cryogenic Permanent Magnet Undulators

HELMHOLTZ
ZENTRUM BERLIN
für Materialien und Energie

Proposed by T. Hara, T. Tanaka, H. Kitamura et al.

T. Hara et al. Phys. Rev. Spec. Topics, Vol. 7, 050702 (2004) 1-6
T. Tanaka et al. Phys. Rev. Spec. Topics, Vol. 7, 090704 (2004) 1-5

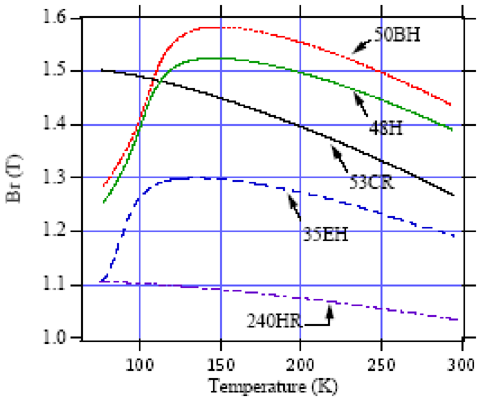

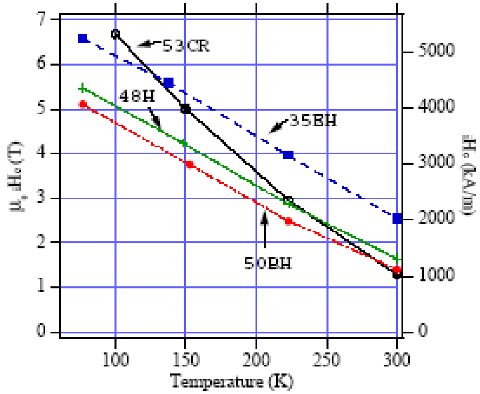

gain in magnetic field
as compared to conventional
in-vacuum undulator: 1.5
mature technology

gain of superconducting ID
as compared to conventional
in-vacuum undulator: 2.0
many open questions

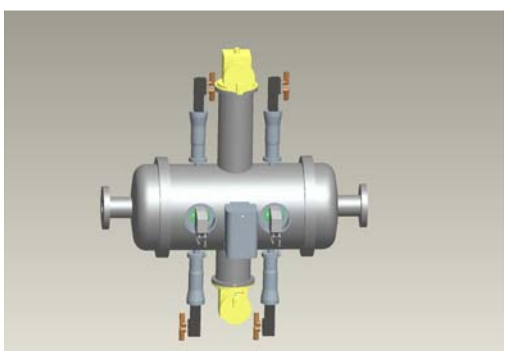

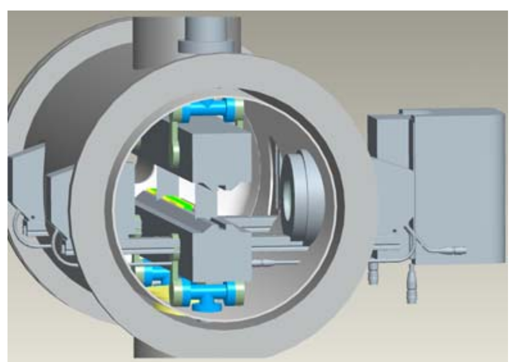

New materials:
- No spin reorientation for PrFeB magnets
- Dy can be used as pole material below the phase transition at 80K saturation magnetization >3Tesla
- Dy diffused magnets (Hitachi)

Cryogenic undulator for table top-FEL application

Magnet Stablity, Magnet Aging I

History of sector 3
downstream undulator at APS

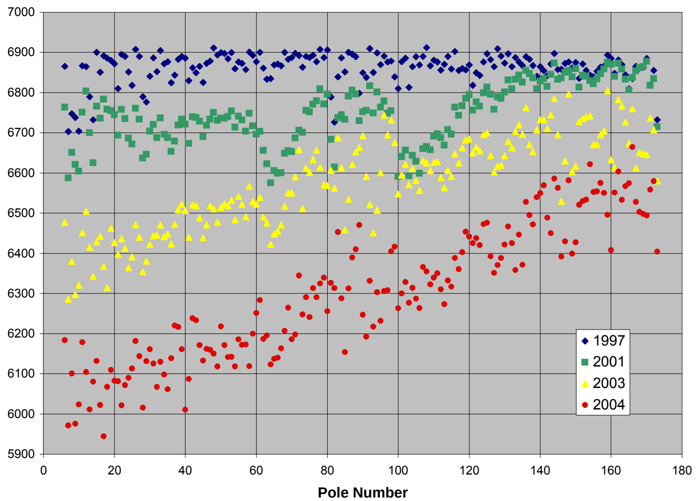

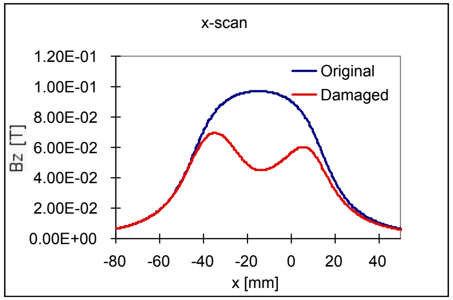

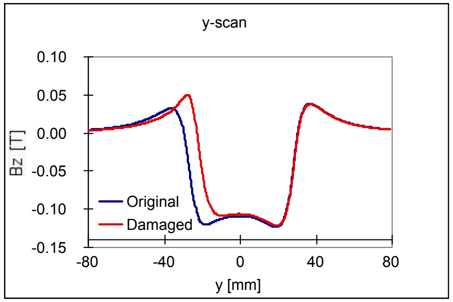

the damages are located close to the e-beam

Field retuning has been done with
- undulator tapering
- magnet flipping or
- remagnetizing of magnet blocks

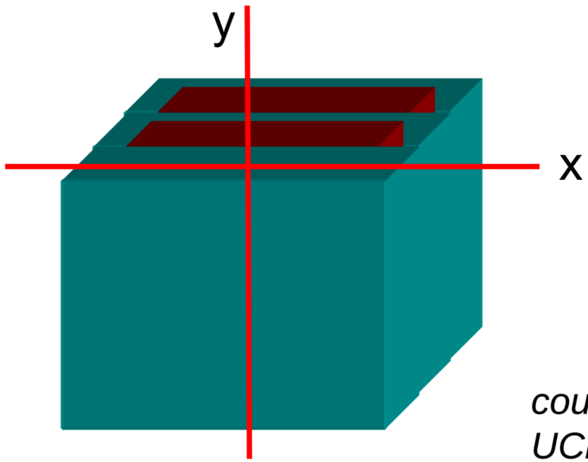

Hall probe scans have been performed at the dismounted magnets along the indicated paths

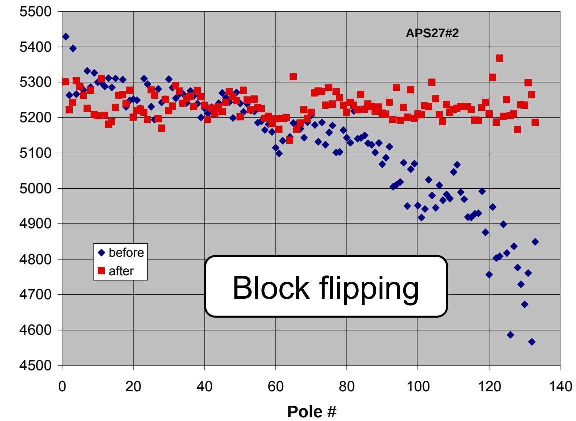

courtesy of L. Moog, APS, Argonne National Lab., operated by UChicago Argonne for US-DOE, contract DE-AC02-06CH11357

Magnet Stablity, Magnet Aging II

Demagnetization has been observed also at other out of vacuum devices:

ESRF *P. Colomp et al., Machine Technical Note 1-1996/ID, 1996*

DESY / PETRA H. Delsim-Hashemi et al., *PAC Proceedings, Vancouver BC, Canada 2009*

In-vacuum applications are even more critical

usage of SmCo or special grades of NdFeB is required

Protection of magnets:

- *Collimator system*
  - dogleg for energy filtering (used in linear accelerators)
  - apertures for off axis particles (LINACS and SR, e.g. SLS-SR)

- *Beam loss detection*

  fast detection
  - scintillators: high sensitivity, medium spatial resolution
  - Cherenkov fibers: medium sensitivity, high spatial resolution

  absolute dose measurements
  - OTDR systems: simple but low dynamic
  - power meter fibers: using several coils: high dynamic

Magnet Stablity, Magnet Aging III

Powermeter fibers

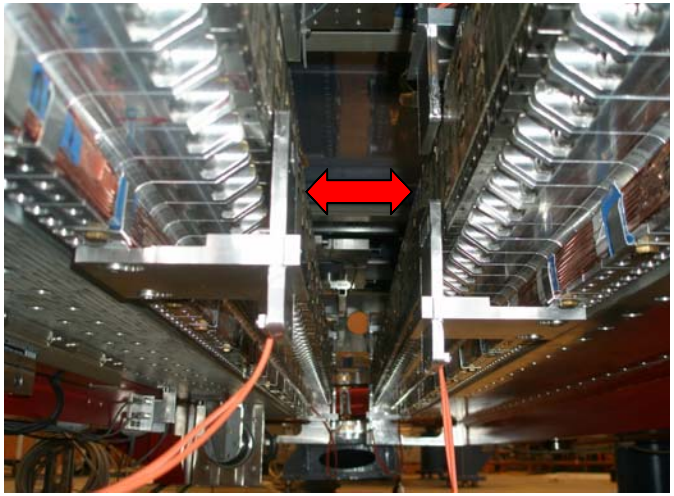

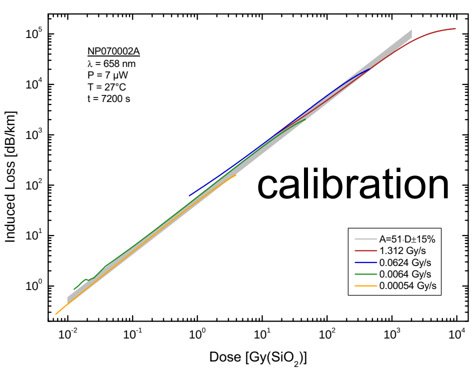

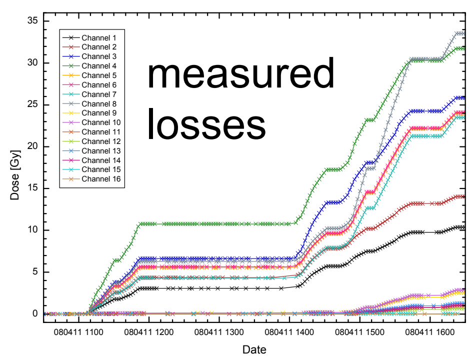

Powermeter fibers as installed at the MAXlab-HZB HGHG-FEL

Cherenkov fibers

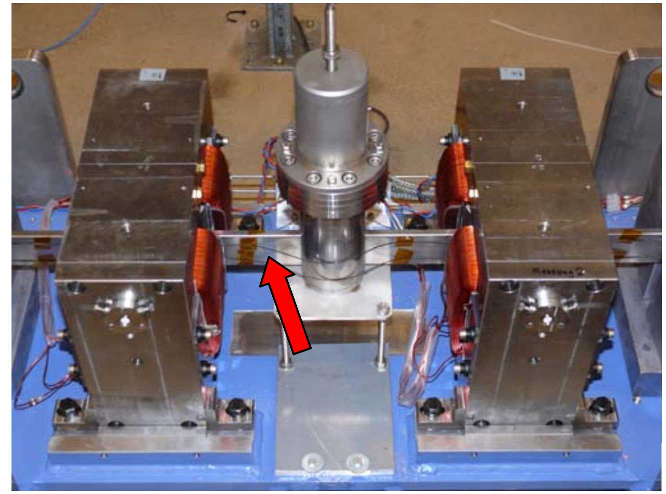

Fibre position	0° losses	45° losses	90° losses
45°	0.00255	0.00341	0.00277
135°	0.00171	0.00186	0.00286
225°	0.00194	0.00189	0.00193
315°	0.00285	0.00206	0.00191

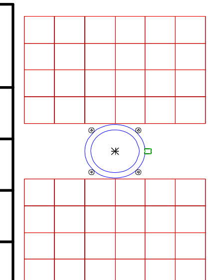

Number of Cherenkov photons per electron

J. Bahrdt et al, Proc. of FEL Conf. Novosibirsk Siberia (2007) pp122-225.
J. Bahrdt et al, Proc of FEL Conference (2008)

Assuming rectangular magnets with $\mu_{par}=1$, $\mu_{perp}=0$

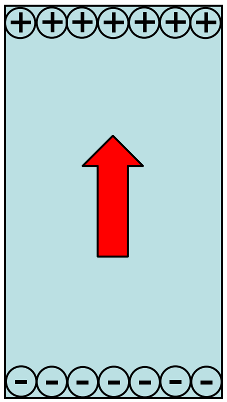

surface charge density at the pole faces

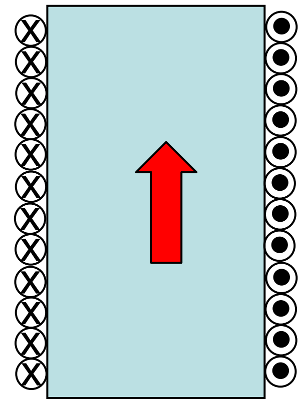

surface currents flowing at the sides of the magnet

$$\Phi(\vec{r}_0) = -\int \frac{\overline{\nabla}' \cdot \vec{M}(r')}{|\vec{r}_0 - \vec{r}'|} dV' = \oiint_{surface} \frac{\vec{n}' \cdot \vec{M}(\vec{r}') dS'}{|\vec{r}_0 - \vec{r}'|}$$

$$\vec{H}(\vec{r}_0) = -grad(\Phi(\vec{r}_0))$$

$$\vec{B}(\vec{r}_0) = \frac{1}{c} \int I d\vec{l} \times \frac{\vec{r}_0 - \vec{r}'}{|\vec{r}_0 - \vec{r}'|^3}$$

$$\vec{B}(\vec{r}_0) = \int \left(\overline{\nabla} \times \vec{M} \right) \times \frac{\vec{r}_0 - \vec{r}'}{|\vec{r}_0 - \vec{r}'|^3} dV'$$

This approach is called CSEM which means either
- Current Sheet Equivalent Method or
- Charge Sheet Equivalent Method

CSEM for a Rectangular Block

Based on these equations the fields can be evaluated by analytic integrations over all current carrying surfaces

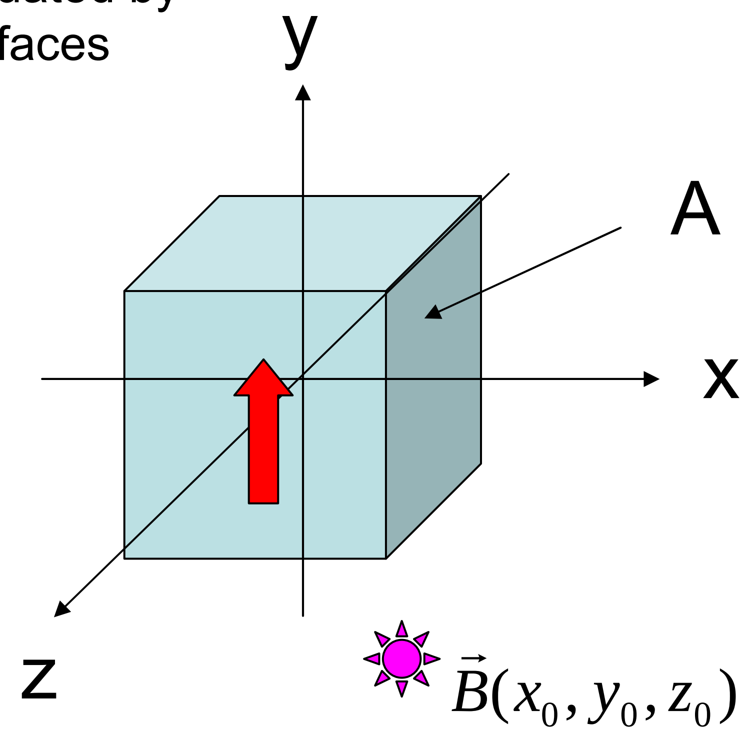

contribution from surface A:

$$B_x = \frac{I}{c} \cdot \iint \frac{y - y_0}{\left((x-x_0)^2 + (y-y_0)^2 + (z-z_0)^2\right)^{3/2}} dz \cdot dy$$

$$B_y = -\frac{I}{c} \cdot \iint \frac{x - x_0}{\left((x-x_0)^2 + (y-y_0)^2 + (z-z_0)^2\right)^{3/2}} dz \cdot dy$$

$$B_z = 0$$

totally:

$$\vec{B}(\vec{r}_0) = \overline{\overline{Q}}(\vec{r}_0) \cdot \vec{M}$$

$$Q_{xx} = \sum_{ijk=1}^{2} (-1)^{i+j+k+1} \arctan\left(\frac{y_j z_k}{x_i \sqrt{x_i^2 + y_j^2 + z_k^2}} \right)$$

$$Q_{xy} = \ln\left(\prod_{ijk=1}^{2} \left(z_k + \sqrt{x_i^2 + y_j^2 + z_k^2} \right)^{(-1)^{i+j+k}} \right)$$

$$x_{1,2}(y_{1,2}, z_{1,2}) = x_c(y_c, z_c) - x_0(y_0, z_0) \pm w_{x(y,z)} / 2$$

(x_c,y_c,z_c) = center of magnet
(x_0,y_0,z_0) = point of observation
(w_x,w_y,w_z) = dimensions of magnet

similarly for all Q_{ij}

Arbitrary Magnetized Volumes Enclosed by Planar Polygones

Similarly, the fields and field integrals from arbitrary current carrying planar polygons can be evaluated

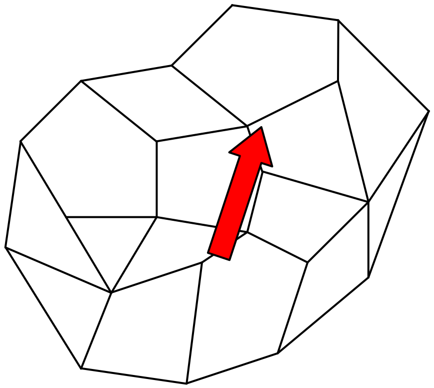

Field

$$\vec{B}(\vec{r}_0) = \overline{\overline{Q}}(\vec{r}_0) \cdot \vec{M}$$

$$\overline{\overline{Q}}(\vec{r}_0) = \oiint_{surface} \frac{(\vec{r}_0 - \vec{r}\,') \otimes \vec{n}\,'_{surface}}{\left|\vec{r}_0 - \vec{r}\,'\right|^3} d\vec{r}\,'$$

Field integral

$$\vec{I}(r_0, \vec{v}) = \int_{-\infty}^{\infty} \vec{H}(\vec{r}_0 + \vec{v}) dl = \overline{\overline{G}}(\vec{r}_0, \vec{v}) \cdot \vec{M}$$

$$\overline{\overline{G}}(\vec{r}_0, \vec{v}) = \frac{1}{2\pi} \oiint_{surface} \frac{[[(\vec{r}\,' - \vec{r}_0) \times \vec{v}] \times \vec{v}] \otimes n'_{surface}}{\left|(\vec{r}\,' - \vec{r}_0) \times \vec{v}\right|^2} d\vec{r}\,'$$

$\overline{\overline{Q}}$ and $\overline{\overline{G}}$ are 3x3 matrices describing the geometric shape of the magnetized cell
They can be evaluated analytically for an arbitrary polyhedron
$\otimes$ denotes a dyadic product

O. Chubar, P. Elleaume, J. Chavanne, J. of Synchrotron Radiation, 5 (1998) 481-484
P. Elleaume, O. Chubar, J. Chavanne, Proc. of PAC Vancouver, BC, Canada, (1997) 3509-3511

Finite Susceptibility Requires Iterative Algorithm

For real magnets: μ_{par}=1.06, μ_{perp}=1.17
Iterative algorithms are required to evaluate the fields.

For pure permanet magnet structures the finite susceptibility lowers the evaluated undulator fields by a few percent as compared to zero susceptibility

$$\vec{B}_i = \sum_{\substack{k=1 \\ k \neq i}}^{N} \overline{\overline{Q}}_{k,i} \cdot \vec{M}_k + \overline{\overline{Q}}_{ii} \cdot \vec{M}_i$$

$$\vec{H}_i = \vec{B}_i - 4\pi \cdot \vec{M}_i$$

$$M_{i-par} = \frac{1}{4\pi} B_r + (\mu_{par} - 1) \cdot H_{i-par}$$

$$M_{i-perp} = (\mu_{perp} - 1) \cdot H_{i-perp}$$

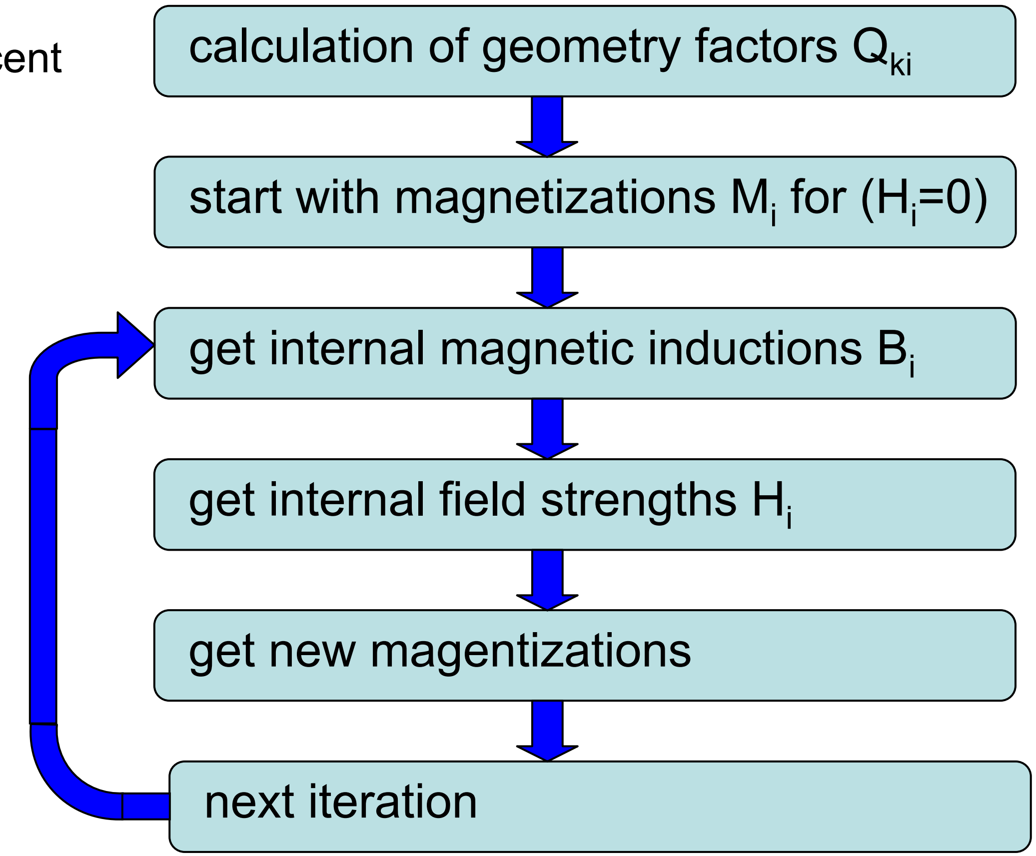

Linear regime

$$M_{par}(H_{par}) = M_r + \chi_{par} H_{par}$$
$$M_{perp}(H_{perp}) = \chi_{perp} H_{perp}$$

Including temperature dependence

$$M_r(T) = M_r(T_0)\cdot(1 + a_1(T - T_0) + a_2(T - T_0)^2 + \ldots)$$
$$H_{cj}(T) = H_{cj}(T_0)\cdot(1 + b_1(T - T_0) + b_2(T - T_0)^2 + \ldots)$$
$$\chi_{perp}(T) = \chi_{perp}(T_0)\cdot(1 + a_1(T - T_0) + a_2(T - T_0)^2 + \ldots)$$

Magnetization Ansatz

$$M(H,T) = \alpha(T)\sum_{i=1}^{3} M_{si}\tanh\left(\frac{\chi_i}{M_{si}}(H + H_{cj}(T))\right)$$

a_i, b_i from data sheet of magnet supplier
M_{si}, χ_i from fit of M(H) curve at T_0 (magnet supplier)
$\alpha(T)$ is determined from

$$M(H = 0, T) = M_r(T)$$

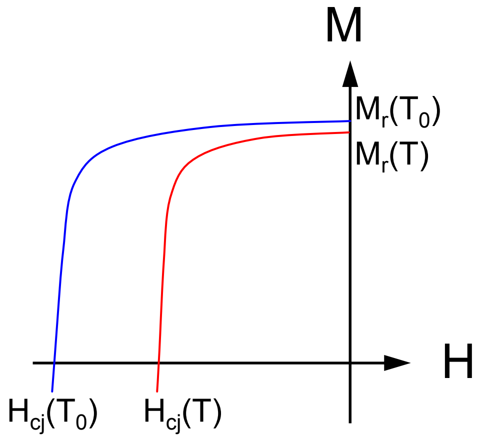

This model has been implemented into RADIA and tested with a real magnet assembly

J. Chavanne et al., Proc. of EPAC, Vienna, Austria (2000) 2316-2318

2-dimensional Geometries

Use complex notation of fields:

$$\vec{B}^*(\vec{z}_0) = B_x - iB_y$$

$$\vec{z}_0 = x_0 + iy_0 = r_0 \cdot e^{i\varphi_0}$$

$\vec{B}^*$ is an analytic function, $\vec{B}$ is not
Cauchy Riemann relations are equivalent to Maxwell equations.
Examples:
Current flowing into the plane:

$$\vec{B}^*(\vec{z}_0) = a\int \frac{j_z}{\vec{z}_0 - \vec{z}} \cdot dx \cdot dy$$

Permanent magnet with remanence $\vec{B}_r$

$$\vec{B}^*(\vec{z}_0) = b\int \frac{\vec{B}_r}{(\vec{z}_0 - \vec{z})^2} \cdot dx \cdot dy$$

$$B_r = B_{rx} + iB_{ry}$$

Optimization using conformal mapping (Halbach)

Easy axis rotation theorem:
rotation of all magnetization vectors by (+α) rotates the field vector B by (- α)

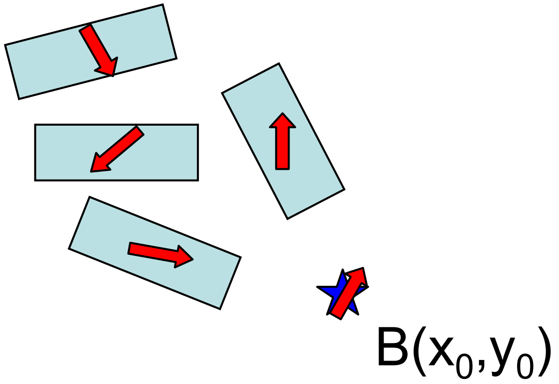

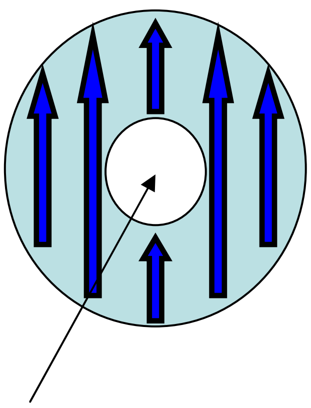

HELMHOLTZ ZENTRUM BERLIN für Materialien und Energie

Halbach type multipoles

General segmented multipole with stacking factor ε≤1
v=harmonic number (v=0 describes the fundamental)
N=order of multipole, N=1: dipole, N=2: quadrupole etc
B_r=remanence
r_1=inner radius
r_2=outer radius
M=total number of magnets per period
α = (N+1)2π/M = relative angle of magnetization between segments

$$\vec{B}^*(\vec{z}) = \vec{B}_r \sum_{\nu=0}^{\infty} \left(\frac{\vec{z}}{r_1}\right)^{n-1} \frac{n}{n-1}\left(1-\left(\frac{r_1}{r_2}\right)^{n-1}\right) K_n$$

$$\vec{B}^* = B_x - iB_y$$

$$\vec{z} = x + iy = r \cdot e^{i\varphi}$$

$$K_n = \cos^n(\varepsilon\pi / M)\frac{\sin(n\varepsilon\pi / M)}{n\pi / M}$$

$$n = N + \nu M$$

$$\left.\frac{n}{n-1}\left(1-\left(\frac{r_1}{r_2}\right)^{n-1}\right)\right|_{n=1} = \ln(r_2 / r_1)$$

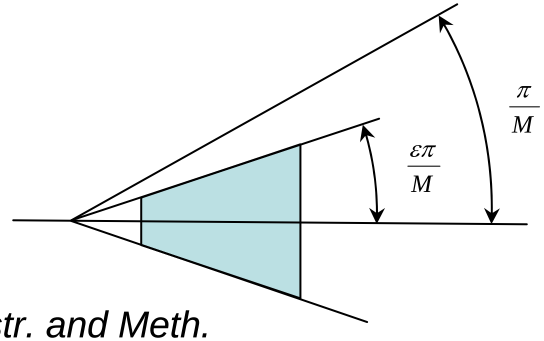

K. Halbach, Nucl. Instr. and Meth. 169 (1980) 1-10

Multipole Magnets for Accelerators II

Example: fundamental of quadrupole: N=2, v=0, stacking factor ε= 1

$$\vec{B}^*(\vec{z}) = \vec{B}_r \frac{\vec{z}}{r_1} 2(1 - r_1/r_2)K_2 \qquad K_2 = \cos^2(\pi/M)\frac{\sin(2\pi/M)}{2\pi/M}$$

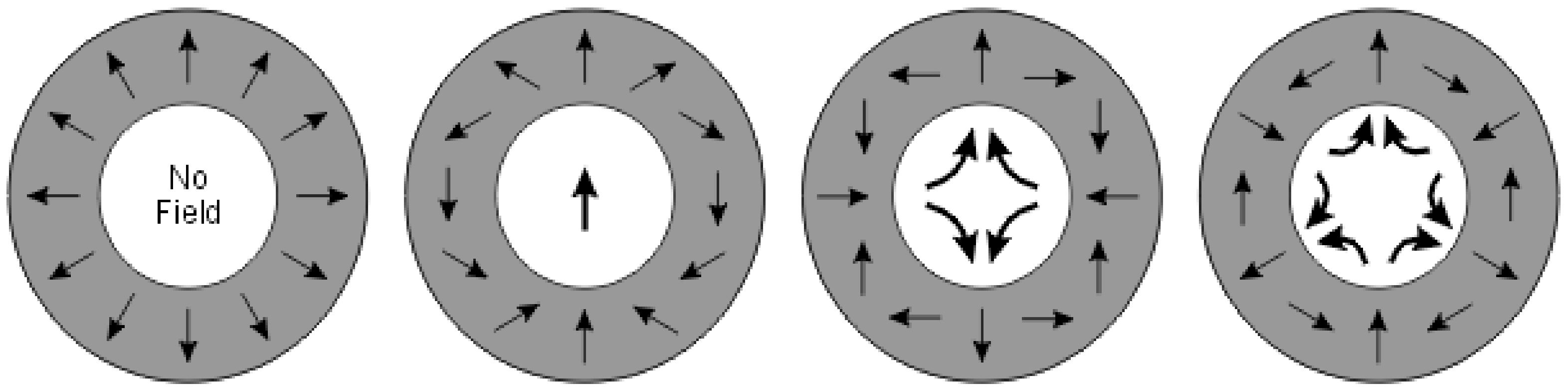

N=0	dipole N=1 M=6	quadrupole N=2 M=4	sextupole N=3 M=3

300T/m
radius: 3.5mm

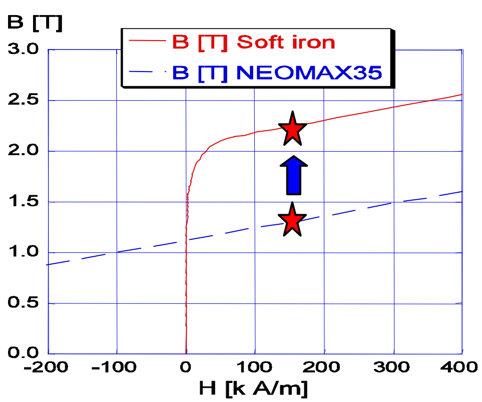

Modified Halbach multipoles include Fe

Y. Iwashita, Proc. of PAC, (2003) 2198-2200

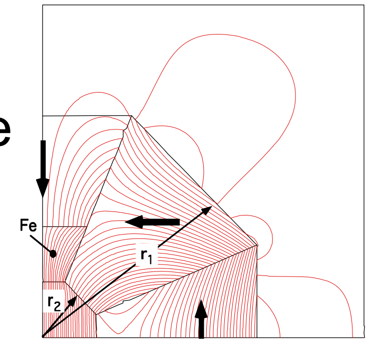

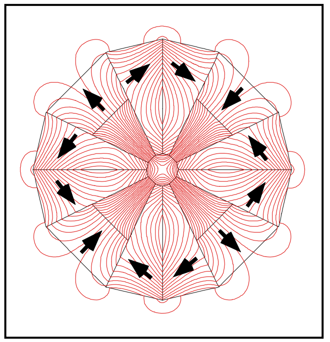

Multipole Magnets for Accelerators III

Continuously adjustable quad for ILC final focus

advantages of permanent magnets versus SC solenoid:
- No vibrations due to liquid HE
- small outer diameter, better geometry for crossing beams

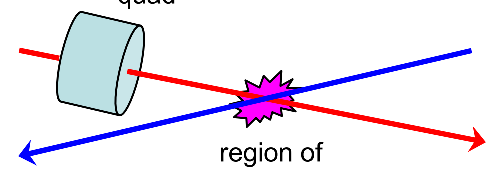

- Effect of a rotated quadrupole is described by a symplectic 4 x 4 matrix M with

$$M^T \Phi M = \Phi \qquad \Phi = \begin{pmatrix} 0 & 0 & 1 & 0 \\ 0 & 0 & 0 & 1 \\ -1 & 0 & 0 & 0 \\ 0 & -1 & 0 & 0 \end{pmatrix}$$

- off diagonal 2 x 2 matrices describe the coupling between planes
- 5 independnet discs can zero the coupling terms and adust the strength
- rotation angles of the five discs are symmetric (see figure)

R. Gluckstein et al., Nucl. Instr. and Meth. 187 (1981) 119-126.

Gluckstern 5 disk singlet

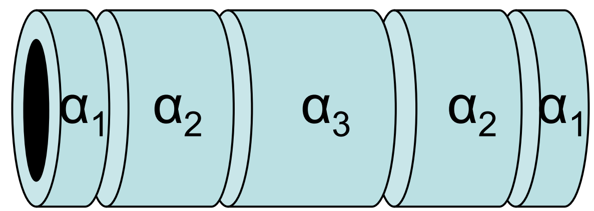

Singlet for ILC final focus
Gluckstern quad
ILC parameters:
Quad gradient: 140 T/m
Inner radius: 12mm
Outer radius: 36mm
Outgoing beam:
4m x 14mrad = 56mm

T. Sugimoto et al., Proc. of EPAC, Genoa, Italy (2008) 583-585.
Y. Iwashita et al., Proc of PAC, Vancouver, BC, Kanada, 2009.

HELMHOLTZ ZENTRUM BERLIN
für Materialien und Energie

Strong focussing ppm quadrupoles (M=3)

for table top FEL undulator: Field gradients up to 500T/m at 3mm inner radius

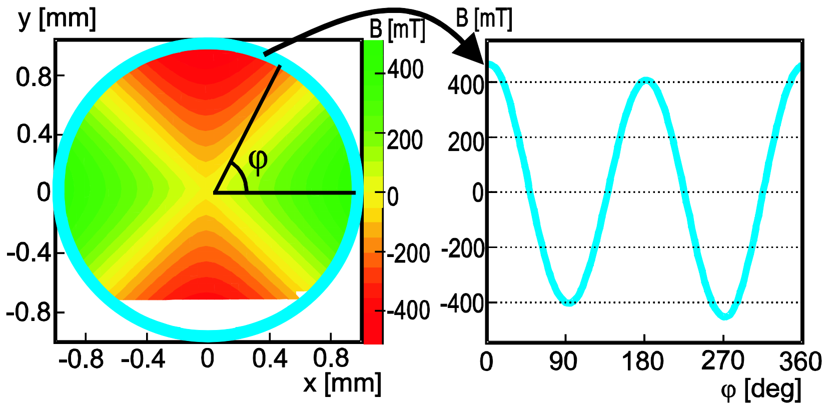

Hall probe measurements

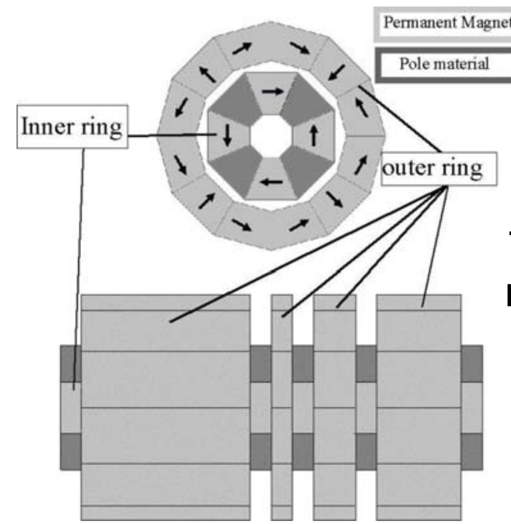

120 T/m
radius 10mm

Binary stepwise PMQ for ILC

Y. Iwashita et al., Proc.of EPAC, Edinburgh, Scotland (2006) 2550-2552.

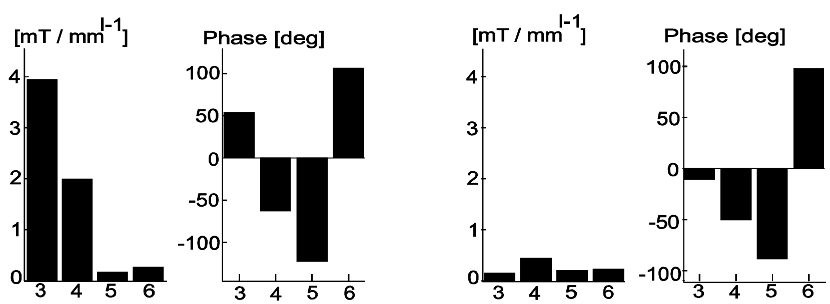

Higher multipole content before (left) and after (right) shimming

T. Eichner et al., Phys. Rev. ST Accel. Beams ***10,*** *082401 (2007).*
S. Becker et al.: *arXiv:0902.2371v3 [physics.ins-det]*

Fermilab 8.9 GeV Antiproton Recycler Ring

3.3 km circumference

344 ppm gradient dipoles
92 ppm quadrupoles
129 powered correctors
material: strontium ferrite

Temperature coefficients:
- remanence of ferrites: -0.19%/deg.
- sat. magnet. of Fe-Ni-alloy: -2%/deg.

temperature dependent flux shunt

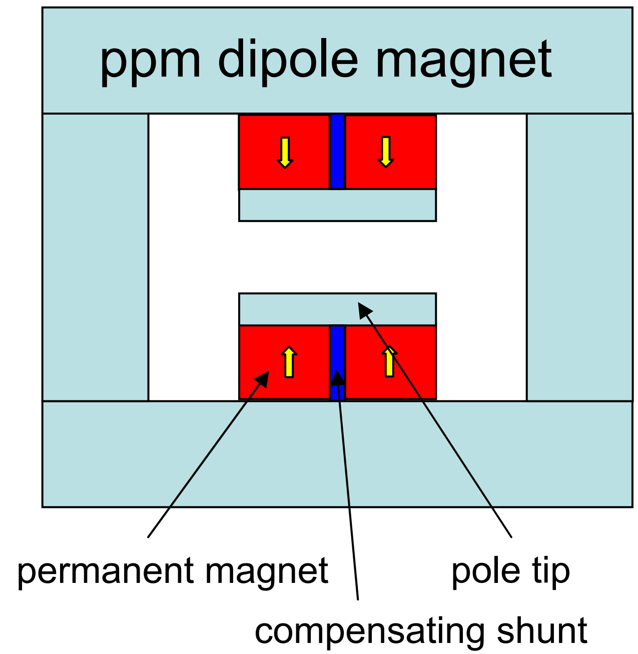

K. Bertsche et al., Proc of PAC (1995) 1381-1383.

LNLS II Proposal I

energy	2.5 GeV
circumference	332 m
number of straights	16
emittance for bare lattice	2.62 nm rad
emittance with damping wigglers	0.84 nm rad
current	500 mA

Permanent magnets to be used:
type: hard ferrite
B_r: 4.0 KG
H_{cj}: 4.5kOe

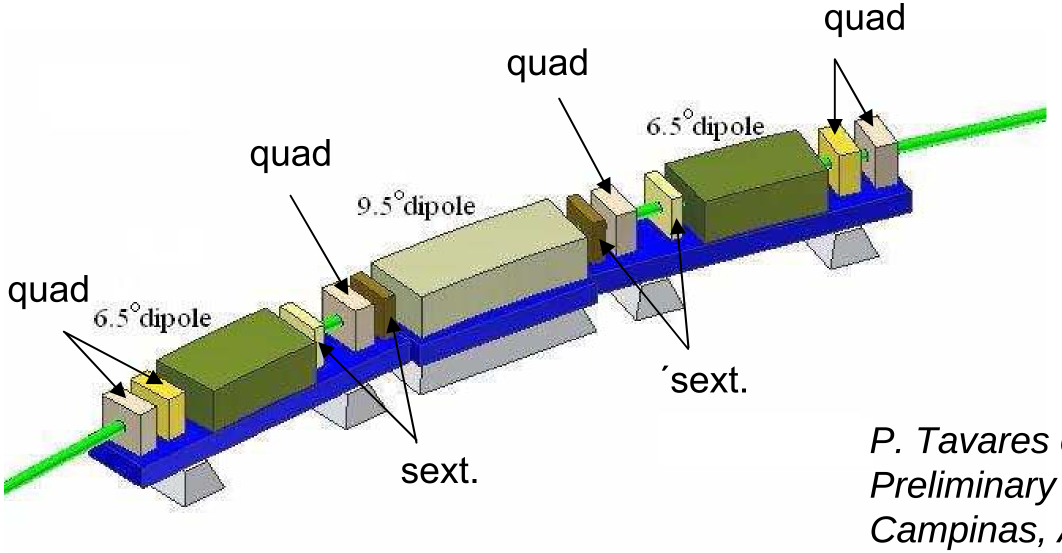

one of 16 cells of the triple bend achromat (TBA) lattice including three dipole magnets and and six quadrupoles

P. Tavares et al, LNLS-2, Preliminary conceptual design report, Campinas, April 2009

LNLS II Proposal II

Permanent magnet **dipole**
including gradient for focussing

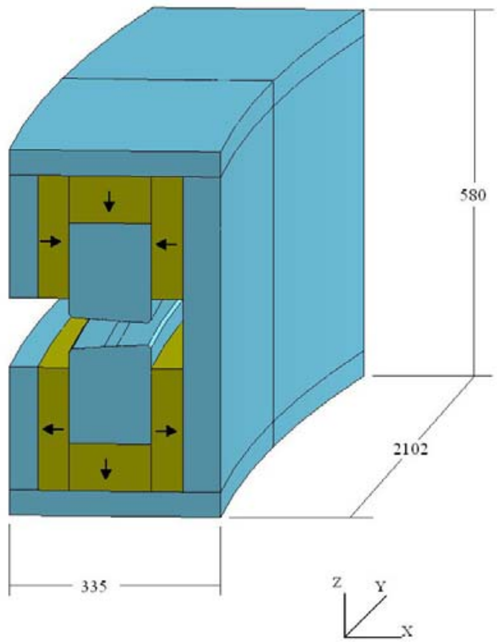

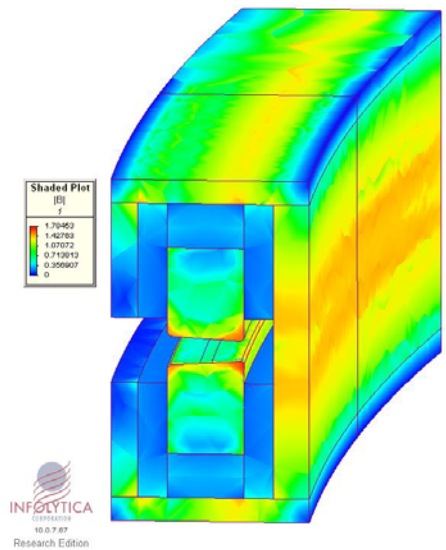

32 x 6.5° dipoles
16 x 9.5° dipoles
peak field: 0.45 T
gradient: 1.25 T / m

Permanent magnet **quadrupole** including trim coils for fine tuning

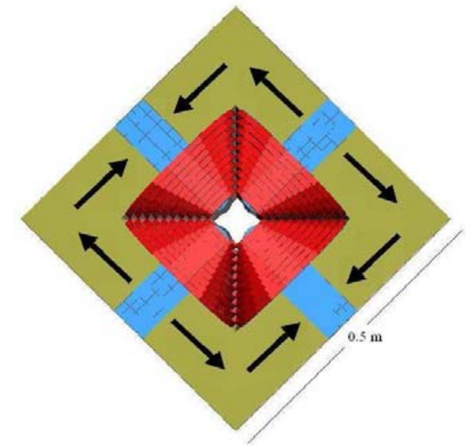

96 quadrupoles
gradient: 22 T / m
integrated gradient:
7.7 T

sextupole magnets will be pure electromagnetic devices